Polyelectrolyte Self-Diffusion: Fluorescence Recovery after Photobleaching of Sodium Poly(styrenesulfonate) in *N*-Methylformamide

Amit Sehgal† and Thomas A. P. Seery*

Polymer Program and Department of Chemistry, Institute of Materials Science, University of Connecticut, Storrs, Connecticut 06269

Received February 26, 2003; Revised Manuscript Received October 8, 2003

ABSTRACT: The influence of added salt on the self-diffusion coefficients (D_{self}) of fluorescein-tagged sodium poly(styrenesulfonate) (SPS) chains in a high dielectric constant organic solvent was measured by fluorescence recovery after photobleaching (FRAP). *N*-Methylformamide (NMF) was chosen since it has a dielectric constant greater than that of water and it was hoped would better solvate the backbone. A new FRAP apparatus was built for the purpose that allowed for data collection of the entire modulated recovery profile of fluorescence intensity. The decay rates of the SPS were determined for multiple bleached grating periods and found to be diffusive in nature. D_{self} was measured for a broad range of added salt concentrations (0−0.1 M) for comparison to the diffusive dynamic modes seen by dynamic light scattering. The self-diffusion coefficients were distinct from both the "fast" and the "slow" modes observed in dynamic light scattering and persisted through the ordinary−extraordinary transition. The slight increase in D_{self} with C_s closely mirrored the "slow" mode diffusion. The slow mode has longer relaxation times as compared to the center-of-mass motion of a single chain, supporting the hypothesis that the slow mode arises from a collective dynamics of large multichain domains.

Introduction

Our light scattering studies[1] of polyelectrolyte dynamics in *N*-methylformamide (NMF) have demonstrated previously that the "extraordinary" behavior of charged polymer solutions was in fact ubiquitous. The study showed that the "slow mode" observed by other research groups in aqueous solutions was present in organic solvents of high dielectric constant for all concentrations of added salt over a range that spanned the expected transition from ordinary to extraordinary behavior. The presence of "extraordinary" relaxations at long times in the dynamic light scattering (DLS) data is often hypothesized to be the result of collective motions of many chains. However, the observed slow mode may also be attributed to self-diffusion (D_{self}) of single chains[2] in an environment with substantially higher friction coefficient. It is therefore imperative to distinguish the slow mode observed through dynamic light scattering from the motions of isolated single chains. In this paper, we extend this investigation of dynamics of polyelectrolyte solution to measurements of self-diffusion of isolated single chains in NMF. A fluorescence recovery after photobleaching (FRAP) apparatus was assembled[3] expressly for measuring the self-diffusion coefficient of sodium poly(styrenesulfonate) in NMF.

The self-diffusion coefficient is the mean-squared displacement of the center of mass of an individual macromolecule,[4] given by

$$D_{self} = \lim_{t\to\infty} \frac{\langle (x(t) - x(0))^2 \rangle}{2t} \qquad (1)$$

Experimental determination of "self-diffusion" or single molecule motion against a surrounding background, also referred to as "tracer diffusion", primarily depends on tracking the motion of labeled molecules. Fluorescence recovery after photobleaching[3,5−9] (FRAP) and forced Rayleigh scattering (FRS)[10−13] are optical techniques that rely on labeling the chain with a photochromic dye. Steady gradient spin echo (SGSE) and pulsed field gradient nuclear magnetic resonance[14−21] (PFGNMR) use the internal magnetic dipoles of the nuclei as tags in a gradient magnetic field to determine translational motion of single chains. Other labeling and measurement techniques include radioactive tracer, Rutherford backscattering,[22] and even some quasi-elastic neutron scattering experiments.[23,24] Oostwal et al.[20,21] have investigated the self-diffusivity of semidilute solutions of sodium poly(styrenesulfonate) in D_2O using PFGNMR as a function of molar mass, polyion concentration, and ionic strength. The requirement of deuterated NMF for similar experiments proved to be a limitation for pursuing neutron scattering or NMR studies in our high dielectric organic solvent.

Since the labeling chemistry for poly(styrenesulfonate) has previously been published, we chose FRAP as a convenient method to determine self-diffusion coefficients in this case. The experiment involves photobleaching a ruled pattern onto a fluorescently tagged polymer solution, gel, film, or any complex matrix with an intense flash of an appropriate excitation wavelength. The dissipation of the pattern is then monitored in real time in terms of the fluorescent intensity from the entire field of view in the optical plane. In FRAP, the highly attenuated reading beam is at the same wavelength as the photobleaching beam,. The FRS experiment, on the other hand, uses an absorption grating created in a tagged polymer solution by interfering beams at a high frequency (and high energy, typically UV). The diffraction pattern from this grating is then monitored by another reading beam. Complications such as thermal absorption that cause dielectric variation contributing to the diffraction, and require-

† Current address: Polymers Division, MS 8542, National Institute of Standards and Technology, Gaithersburg, MD 20899.
* To whom all correspondence should be addressed.

10.1021/ma034251e CCC: $25.00
Published on Web 11/27/2003

ment of optical clarity, also influenced the decision to build an apparatus based on the FRAP technique.

Apparent self-diffusion coefficients have also been measured by DLS in the semidilute regime. Amis et al.[2] observed long time relaxations in semidilute solutions of neutral chains and attributed them to the self-diffusion coefficient. Confined by entanglements, the chains are thought to translate by reptation resulting in a slow center-of-mass motion. They measured slow diffusion coefficients that scaled with polymer concentration, $D_{slow} \sim C_p^{-1.75}$, and with molar mass, $D_{slow} \sim M^{-2}$, that were in accordance with scaling theory, barring some deviations at the extremes. The observation of this long time relaxation that scales as self-diffusion is expected for neutral chains and could lead to the hypothesis that the "slow mode" in DLS data on polyelectrolytes could be due to self-diffusion. Our FRAP measurements provide a test for this hypothesis.

The influence of ionic strength on self-diffusion of polyelectrolytes in aqueous solutions measured by FPR and PFGNMR is now extended to a high dielectric organic solvent. Zero et al.[5] and Ramsay et al.[25] have studied aqueous solutions of poly-L-lysine with added KCl, resulting in identical results from the modulation-based and the spot-bleaching techniques for photobleaching recovery. Yu and Russo[26] have studied generation 5 and generation 3 PAMAM dendrimers, and Oostwal has conducted PFGNMR studies[20,21] on the self-diffusion of SPS as a function of ionic strength in an aqueous solutions. To our knowledge, this is the first study that extends this inquiry into an organic solvent.

The FRAP Experiment. The FRAP experiment is based on the modulation technique first suggested by Lanni and Ware.[3] A Ronchi ruling is placed in the optical path and imaged on to the sample using a microscope operating in the reflective mode. A high-intensity laser beam writes the grating pattern on the sample by photobleaching the fluorescent tracer molecules with an image of the ruled pattern. The pattern is observed using modulation detection by translation of the ruling in the path of a collinear highly attenuated beam at the same wavelength. This periodic tracer gradient can be expressed for position x at time 0 as a Fourier series, for the fluorescent tracer concentration, "c" ; bleach depth, Δc; and grating constant $K = 2\pi/L$, corresponding to a linear period L. This is given by the equation[3]

$$c(x,0) = \left(c_0 - \frac{\Delta c}{2}\right) + \frac{\Delta c}{2}\frac{4}{\pi}\sum_{\substack{\text{odd}\\ n>0}}^{1}\frac{1}{n}\sin nKx \qquad (2)$$

Only motions of the fluorescently labeled molecules that are perpendicular to the grating will result in the dissipation of the pattern over time as labeled molecules undergo a center-of-mass translation between bleached and unbleached regions. Modulation detection by a reading beam at the same wavelength and a lower intensity gives a photocurrent profile for the dissipation of the bleached grating:

$$F(t) = \frac{1}{2}\alpha I_0\left\{\left(c_0 - \frac{\Delta c}{2}\right) - \left(\frac{\Delta c}{2}\right)\frac{8}{\pi^2}\sum_{\substack{\text{odd}\\ n>0}}^{1}\frac{1}{n^2}\,e^{-DK^2n^2t} \times \cos(nKvt)\right\} \qquad (3)$$

where D is the self-diffusion coefficient of the fluorescing species, I_0 is the incident beam intensity, α is the fluorescence emission efficiency, and the pattern velocity is denoted as v . In principle, the Fourier nature of eq 3 could provide the opportunity to extract multiple terms from the data so that several effective grating spacings could be obtained in a single experiment. However, in practice, the second term, $n = 3$, is nearly an order of magnitude smaller with an order of magnitude faster decay. At present, the noise in the data will not allow for reliable extraction of the $n = 3$ Fourier component, and so we have fit our data using only the $n = 1$ term in the series. This sinusoidal wave with its superposed exponential decay uses the self-diffusion coefficient as the only adjustable parameter. Different grating sizes and objective magnifications alter the period of the pattern and the time scales of motion probed.

Pattern photobleaching has several distinct advantages over the spot-bleaching experiments used earlier. The spot-bleaching technique, though one-dimensional in the radial sense, is subject to errors due to sample drift over long time and strong dependence on the bleached spot depth and its three-dimensional profile, especially with high numerical apertures for small length scales of diffusion. In our instrument we examined samples using bleach depths between 5 and 20%. Although the use of shallow bleaching is an advantage of FRAP, we did not optimize our experiments for this parameter, and our measurements did not show any dependence on bleaching depth. The use of a pattern simplifies the analysis by restricting the experiment to a single coordinate axis and also allows the operator to easily vary the length scales and the experiment time for measuring slow mobilities. The modulation technique makes the experiment insensitive to dc drifts and photobleaching by the reading beam.

Experimental Section

The FRAP experiments on our model polyelectrolyte system, sodium polystyrenesulfonate in *N*-methylformamide, are conducted on a new instrument, assembled at the University of Connecticut for this purpose. The polymer is lightly tagged with a fluorescein derivative fluorophore. All measurements were performed at $\lambda = 488$ nm for three grating sizes of 50, 100, and 200 lines/in. The actual grating periods (L) used for the calculations were determined by optical micrometry to be 50, 25, and 12.5 μm with corresponding grating constants, K, of 628, 1256.6, and 2513 cm^{-1}. A single microscope objective (10×) was chosen for all the measurements to be on an experimentally convenient time scale. The instrumentation was modeled after the experimental designs of Bu,[7] Lanni,[3] and Zero.[4] The detector was a 1.125 ft HC 124-03 Hamamatsu photon counting detector assembly, and the apparatus was controlled by a PC equipped with a CyberResearch counter/timer card (CYCTM-05) and digital I/O card (CYRDIO-24H) that allowed programmable 16 bit counters to easily collect the 1 MHz signal from the PMT.

Scheme 1. Synthesis Scheme for Tagging the SPS[a]

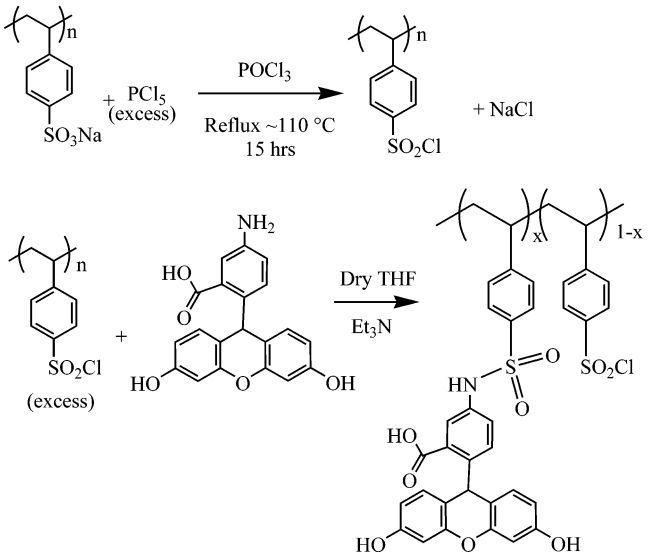

[a] Use of the PCl_5 gives high yields. The fraction 0.0074 represents quantitative tagging. Actual levels are expected to be lower.

Synthesis of Fluorophore-Tagged Polymer. SPS, from the same batch as used in our previous dynamic light scattering studies,[1] at a molecular weight of 200 000 g mol^{-1}, was modified with a very low concentration of fluorescein labels. The labeling procedure is outlined in Scheme 1. The scheme involves converting the sodium sulfonate moieties along the backbone to sulfonyl chlorides, attaching the dye to the chloride as the fluoresceinamine derivative, and then hydrolyzing the remaining sulfonyl chlorides back to their sulfonic acid form. Molarities are given in terms of monomer units. The chlorination was performed with a $PCl_5/POCl_3$ mixture.[27] A molar ratio of 1:4:23 for styrenesulfonate/PCl_5/$POCl_3$, respectively, in the mixture has been shown to be the most effective. PCl_5 (4 g) was refluxed with 16 g of $POCl_3$ in a 200 cm^3 round-bottom flask at ~110 °C. The $POCl_3$ acts as a solvent for the PCl_5. The SPS (450 mg) was added to this boiling mixture with stirring for 15 h. The reaction was quenched by slowly adding H_2O to the suspension. The slightly beige precipitate was filtered and washed with copious amounts of water. This precipitate was dried on a vacuum line overnight to remove all traces of water. A dry weight of 380 mg, corresponding to an 80% yield, was obtained. The polymer in the sulfonyl chloride form (200 mg, 1 mmol) was then suspended in dry tetrahydrofuran (THF) at room temperature. A solution of 10 mg (0.03 mmol) of fluoresceinamine (isomer I, purchased from Aldrich) and triethylamine (0.876 g, 8.64 mmol) as in the procedure of Sohn[28] was made in 5 mL of THF. The solution was heated to ensure complete dissolution. A 1.1 g portion of this solution was then added to the sulfonyl chloride suspension (corresponding to an added tag content of 0.0075 mmol), giving an added tag concentration of 0.75%. The reaction is immediate and is indicated by a change in color of the precipitate. The THF was removed under vacuum, and the sample was allowed to dry. This dry, labeled, sulfonyl chloride functionalized polymer was hydrolyzed by boiling with 10 mL of 2% NaOH solution for 20 min to convert the unreacted sulfonyl chloride to sulfonate. The suspension turns clear, indicating complete hydrolysis and dissolution. The suspension was then neutralized with HCl. This solution, which has a high salt content from the neutralization, was then dialyzed against deionized water in 5K Da membranes for 24 h. Bio-Rad AG 501-X (8) mixed bed deionization resin was added to the dialysis bath to accelerate the process and ensure removal of all ions. The fluoresceinamine-tagged poly(styrenesulfonate) solution is now in an acid form. The dialyzed solution was then freeze-dried and subsequently stirred with THF for 6 h to ensure removal of all unattached fluoresceinamine. The polymer was centrifuged out of the THF suspension and vacuum-dried again overnight to remove all traces of THF. The acid form was then titrated with a dilute NaOH solution to the conductometric end point to provide sodium counterions for the sulfonate groups. The fluoresceinamine-labeled sodium poly(styrenesulfonate) (FASPS) was freeze-dried and stored under dry conditions.

Sample Preparation. NMF purchased from Aldrich was too conductive for our purposes and was refluxed and then vacuum-distilled over barium oxide prior to use. A Vigreaux column was used to counter bumping of BaO. The distillate had a conductivity of only 20 μmhos and was deemed suitable. Sodium chloride used for the experiment was analytical grade and dried in an oven prior to use. Solutions of the FASPS were then made at a polyion concentration of 0.04 mol L^{-1} at various added salt levels. These polyion concentrations are identical to our previous DLS studies.

The tagged FASPS solutions in NMF were loaded into the Vitrodynamics microchannel slides by capillary action. The data presented were taken only in the 0.2 mm × 4 mm × 5 cm slides. The slides were washed with soap solution, soaked and thoroughly rinsed with deionized water, and then washed with acetone and methanol, before being dried in an oven for 24 h prior to use. The scintillation vials for making the solutions were also similarly treated prior to use. The ends of the slides were then sealed with fresh paraffin wax to exclude moisture uptake. The measurements were made immediately after loading.

Data Analysis. The data acquired show the complete time evolution of the recovery profile including the oscillations as shown in Figure 1 and the dc recovery profile of the baseline. The dc recovery is like spot-bleaching recovery due to the replenishing of the illuminated region with fluorophore-tagged SPS via diffusion from the surrounding area. In our experiments the use of NMF as solvent affects the bleachability of the fluorescein; this required bleaching times as long as 2 s, and this is far shorter than the dc recovery times that are on the order of 300 s. Though there is information in the radial, one-dimensional, recovery profile, the analysis is complicated by sample drift, bleaching depth, and profile shape factors. There are treatments to address these issues, which we avoid at this time by using the modulated approach. The dc recovery baseline was determined by a single-exponential least-squares fit which automatically compensates for the contributions from the ac component. The normalized fluorescence intensity of the ac component was evaluated by

$$F_{ac}(t) = \frac{F(t)}{F_{dc}(t)} - 1 \tag{4}$$

Further analysis of the ac data uses a software equivalent of the peak voltage detection electronics used by other workers. The positive and negative recovery profiles were separately evaluated by a macro compiled in IGOR, a data analysis package. The macro code first evaluates the zero level crossings for the ac component and then, on the basis of a positive or negative going signal, finds the peak between consecutive crossings and stores the respective profiles in separate vectors. The data in Figure 1 do show imperfections or "chatter" in the recovery profiles attributed to mechanical vibrations in the motion table for the Ronchi rulings. This noise in the signal is complementary for the positive and the negative recovery profile. A moving average of the combined positive and the negative signals automatically compensates for this chatter. This decay envelope, $E(t)$, then generated is fit to a single exponential to yield the self-diffusion coefficients from the simple equation

$$E(t) = E(0)e^{-DK^2t} \tag{5}$$

where $K = 2\pi/L$ represents the grating constant for the line period, L.

Results and Discussion

The self-diffusion coefficients of sodium poly(styrenesulfonate) in *N*-methylformamide were measured by

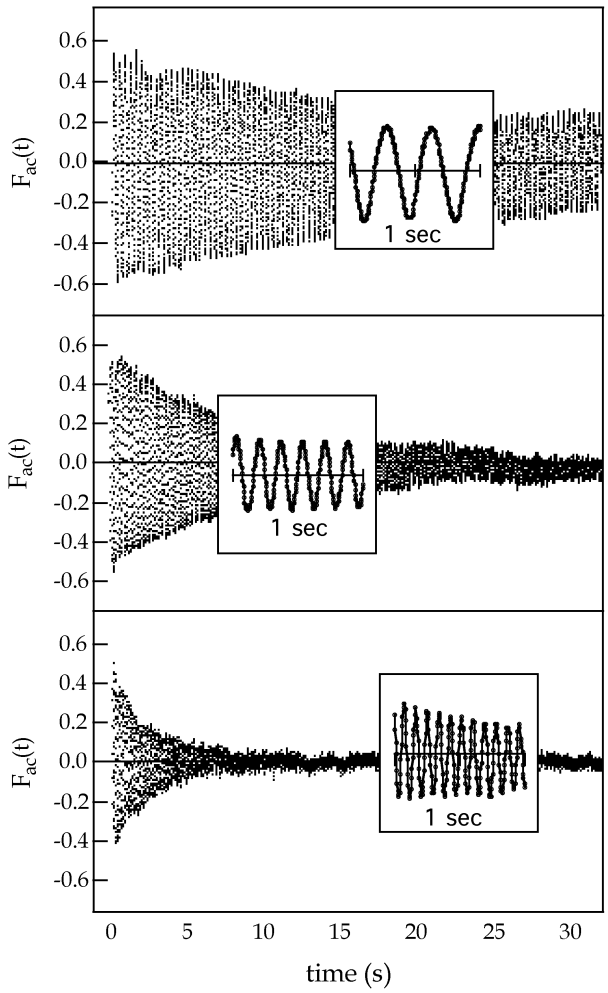

Figure 1. Typical decay profile data for the ac component of normalized fluorescence intensities. The data show the complete recovery process using different gradient periods, L = 50, 25, and 12.5 μm (a−c). Polyion concentration is 0.04 mol L^{-1} at zero salt. Insets are 1 s snapshots showing the oscillations.

fluorescence recovery after photobleaching (FRAP) experiments. The experiments were conducted on the same monodisperse polymer ($M_w = 2 \times 10^5$) at monomer molar concentration of ~0.04 mol L^{-1} as used in the previous DLS study.[1] Data were acquired for a range of added sodium chloride concentrations from 0 to 0.087 mol L^{-1}, spanning the o−e transition. Since FRAP requires modificaton of the polymer by an attached photochromic dye, one must verify that the labeling level is low enough that the dynamics are otherwise unperturbed. This polymer, though modified by lightly tagging with the fluorescein dye (referred to as FASPS), has the same cooperative diffusion coefficient as the native polymer at high added salt (C_s = 0.15 M) as confirmed by DLS measurements. Intrinsic viscosity and DLS measurements on poly(γ-benzyl α,L-glutamate) conducted by Bu and Russo et al.[8] showed insignificant differences in dynamics for label densities less than 1% of the monomer subunits. Forced Rayleigh scattering measurements[12] on center-labeled and end-labeled polystyrenes in tetrahydrofuran demonstrated that the self-diffusion coefficients are independent of the position of the tags along the polymeric backbone and label concentration per chain. These experiments support the use of the random tagging as long as the overall label content per monomer is low.

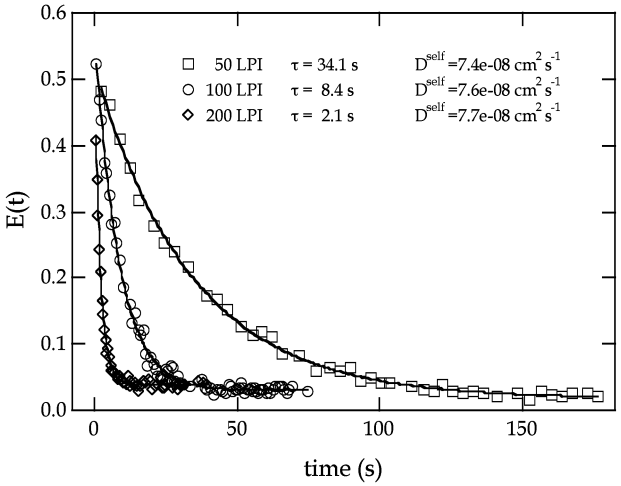

Figure 2. Decay envelopes for the data shown in Figure 1 from the peak amplitudes of the triangle waves. A single-exponential fit describes the data, showing faster decays for finer gratings with reduced length scales. C_p = 0.04 M; C_s = 0.

Typical real-time evolution of the fluorescence decays is plotted as normalized intensities in Figure 1. The raw data shown are for zero added salt at different grating constants ($K = 2\pi/L$) of 628, 1256, and 2513 cm^{-1}, corresponding to the 50, 100, and 200 lines/in. Ronchi rulings, respectively. The envelope of the photocurrent profile decays rapidly with decreasing grating period, as expected. The decay rate ($\Gamma = \tau^{-1} = DK^2$) is inversely proportional to the square of the grating period and yields a value of the self-diffusion coefficient of D_{self} = (7.67 ± 0.15) × 10^{-8} cm^2 s^{-1} (Figure 2). The standard uncertainties are all calculated for the exponential fits.

Though the data were acquired for a total of 3 min, they are shown over 30 s to effectively illustrate the decays. Our experimental profile is different from that used by previous workers since the complete photocurrent profile is generated rather than just the envelope of the decays. Fourier analysis of the full modulated profile with further refinements in instrumentation could be extended to probe coupled dynamics of two self-diffusing species or to detect multiple dynamic modes. However, the data presented below were treated to the traditional analysis of the decay envelope and detected a single self-diffusive species for this system. The photon counts in the following data were generated for a 4 ms sampling time. The inset 1 s snapshots (Figure 1) of the PMT signal show the oscillations of the fluorescence intensity as the illumination pattern and the photobleached pattern fall in and out of phase. The data were acquired at a constant motor speed of the motion table and show twice the frequency of the oscillations with half the grating period. It also gives a measure of the velocity of the illumination pattern at the sample stage for the given optical configuration, which is a possible fitting parameter in eq 3. In this case, it is calculated to be 0.14 mm s^{-1}.

Another feature of the data is that the decays for the finest grating sizes appear to decay to noise at zero, while such is not the case for the largest grating size even when viewed at very long times. The oscillations survive even at long times. The image of the largest 50 LPI grating when viewed through the eyepieces has only five rulings (dark and bright) for a circular spot size of 0.25 mm. A rectangular "bright" ruling when viewed against the curvature of the spot shows a substantial

reduction in the illuminated area for that ruling. As this moves across the spot, the total illuminated area for the spot changes in a sinusoidal fashion. This contributes a small-amplitude oscillation to the baseline and was verified by collecting data with the moving grating without the photobleaching phase.

The envelope of the decays was determined, as described previously, with the averaged positive and the negative recovery profiles. Figure 2 shows the decays, $E(t)$, for the raw data in the previous plot for the three grating sizes against experimental time. The data points have been smoothed, and for clarity, only every 10th point is displayed. The decays again highlight the sharply decreasing relaxation times with reduced length scales for diffusion. The single-exponential fits overlaid on the data completely describe the decay profile. As discussed before, the oscillations for the larger grating periods survive to long times. The peak detection routine could not determine any modulations in the baseline after 30 s for the 200 LPI grating. They survive to 75 s for the 100 LPI ruling and the entire duration of the experiment for the largest grating size. The diffusion coefficients calculated independently for each of the decays as shown in the figure are in good agreement with each other within the standard error for the measurements ($D_{self} = (7.55 \pm 0.13) \times 10^{-8}$ cm^2 s^{-1}).

The slow mode observed in the dynamic light scattering data has been attributed to the presence of multichain domains. This raises the possibility of another slowly diffusing entity in solution in addition to the single chain self-diffusion. The decay envelope, $E(t)$, should, in this event, be biexponential. The relatively long time scales for domain motion, when compared to the self-diffusion of single chains, make for a dynamic system in which the bleached and the unbleached chains are constantly exchanging between domains by self-diffusion. Bleached or unbleached domains would cease to exist on a shorter time scale than their relaxation processes. The decay would therefore be single exponential with almost all the single chains existing in domains.

The influence of added salt concentration on the self-diffusion in context of the DLS measurements of the two dynamic modes was then investigated. The ionic strength of the FASPS solutions in NMF was varied over 2 orders of magnitude across the calculated o−e transition. Figure 3 shows a stack plot of the raw data for three salt concentrations differing by a factor of 30 at C_s = 0.003, 0.00176, and 0.087 M. These data shown here were acquired at $K = 2513$ cm^{-1}, a sample time of 4 ms, and at the same velocity setting of the motion table for comparison. The decay data reflect a gradual increase in the self-diffusion coefficients with substantial increase in ionic strength. This change is expected and mirrors the changes seen for aqueous solutions of poly-L-lysine by Zero and Ware[5] and by Ramsay and Schmitz.[25] At the higher added salt levels, the signal amplitude is apparently weaker, but this is attributed to the faster relaxation times at high salt and the delay between the bleaching phase and the start of the data acquisition. This is due the current experimental constraint of requirement of the solenoid for the PMT shutter to be held at a high voltage for it to open the shutter. The nonrepresentative anomaly seen in the data at $C_s = 0.003$ M at $t = 28$ s, and a vestige of the same seen in the baseline at 25 s for $C_s = 0.0176$ M, is the inevitable grating turnaround point for the motion

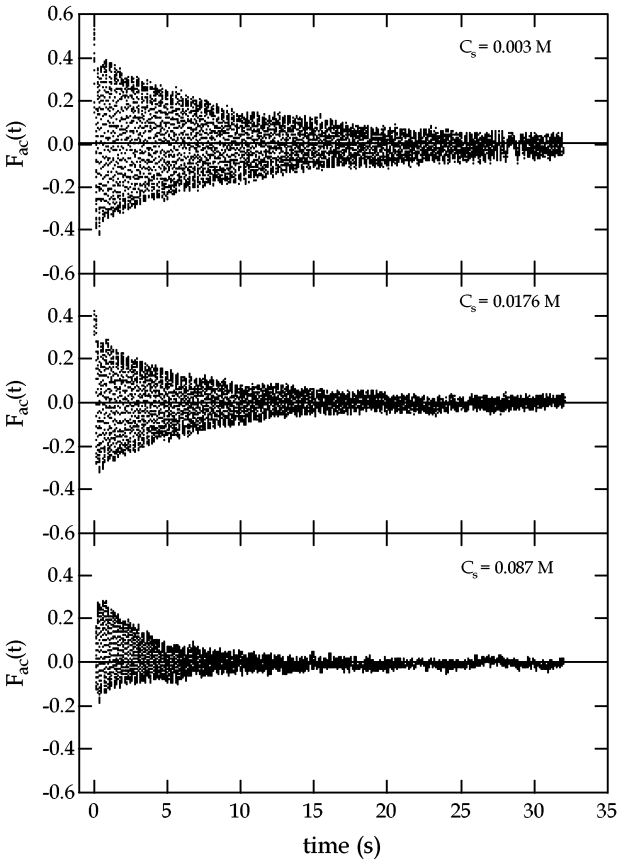

Figure 3. Normalized fluorescence intensities for three added salt concentrations and at grating constant $K = 2513$ cm^{-1}. Data show faster decays, i.e., enhanced diffusion, at higher ionic strengths.

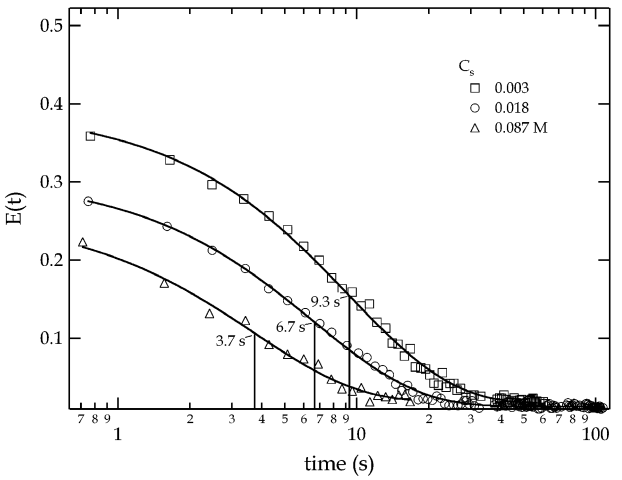

Figure 4. Semilog plot of the decay envelopes for the data in Figure 3 at different added salt levels. $K = 1256$ cm^{-1}. Fits to exponential decays yield the relaxation times shown in the figure.

table. These anomalies are typical in all decay profiles and were excluded from the data analysis.

The decay envelopes, $E(t)$, for the data in Figure 3 were determined for the three salt concentrations and are plotted against time on a logarithmic scale in Figure 4 to accentuate the change in the relaxation time. The single-exponential fit describes the data accurately. Relaxation times calculated from the fits decrease from 9.3, to 6.7, to 3.7 s, corresponding to D_{self} values of $(1.7 \pm 0.1) \times 10^{-7}$, $(9.5 \pm 0.1) \times 10^{-8}$, and $(6.9 \pm 0.1) \times 10^{-8}$

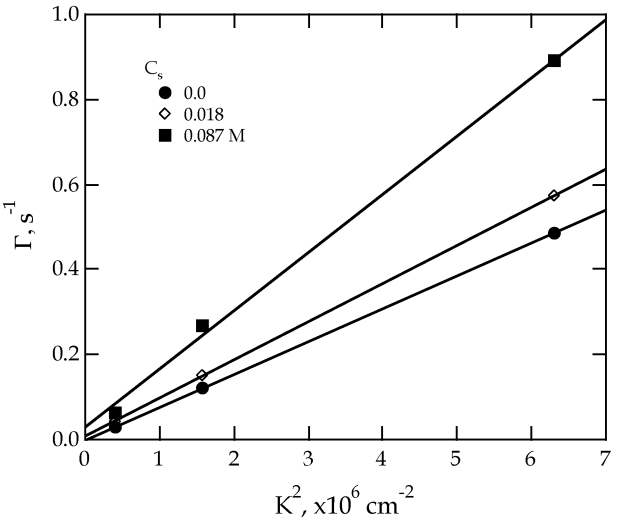

Figure 5. Relaxation rates from the exponential fits at three grating spacing for three added salt concentrations show a linear dependence with K^2.

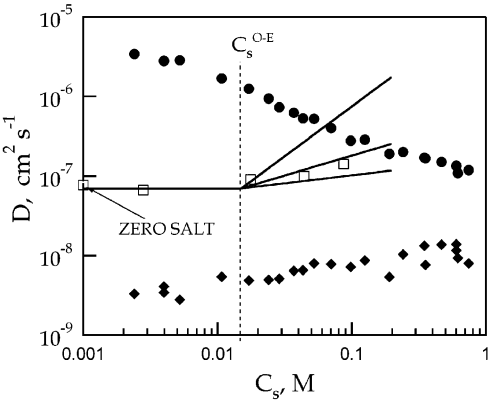

Figure 6. Self-diffusion coefficients for SPS (□) measured by fluorescence photobleaching recovery superposed on the cooperative diffusion coefficients for the fast mode (●) and the slow modes (◆) as seen by DLS. The data spans the o−e transition. $C_p = 0.04$ M for the entire data set.

$cm^2\ s^{-1}$ with increasing salt concentration. These numbers, however, correspond to the relaxation rates for a single tracer gradient period. These measurements were extended for all ionic strengths for a range of grating constants. Figure 5 shows the determined Γ values against the optical K^2 for $C_s = 0$, 0.0176, and 0.087 M. The straight-line dependence through the origin, as given by eq 5, is purely diffusive and completely descriptive of the periodic tracer gradient recovery. The zero intercept points to irreversible chemical photobleaching of the dye and no convection or a thermal gradient due to the high-intensity photobleaching process. The slope of the line gives a measure of the self-diffusion coefficients averaged over a range of K^2, corresponding to the increasing added salt concentrations.

This analysis is extended for all the five samples studied, spanning the range of ionic strengths, and the data are plotted in Figure 6 along with our previously reported dynamic light scattering results. The comparison of the self-diffusion data with the slow and the fast diffusive modes of SPS in the dynamic light scattering data in *N*-methylformamide underscores that they are an order of magnitude larger than the slow mode and an order of magnitude slower than the observed fast mode at low salt. Even for neutral chains the self-diffusion is generally slower than the cooperative diffusive dynamics of the chain segments. The self-diffusion data are distinct from either dynamic mode seen in DLS studies. The slow mode possesses a longer time scale than the center-of-mass motion of a single chain, supporting the hypothesis that the slow mode arises from a collective dynamics of large multichain domains. D_{self} increases gradually with ionic strength and tends toward the fast mode diffusion coefficients ascribed to single chain hydrodynamic motion at high salt concentrations after the "o−e transition". The self-diffusive trend does not undergo a dramatic transition at the calculated C_s^{o-e}, suggesting that there is no catastrophic change in chain conformation. The data show a 2-fold increase in the measured diffusion coefficients, from 7.7×10^{-8} $cm^2\ s^{-1}$ at zero salt to 9.0×10^{-8} $cm^2\ s^{-1}$ at 0.02 mol L^{-1} to 1.4×10^{-8} $cm^2\ s^{-1}$ at 0.087 mol L^{-1} of added salt. This corresponds to a decrease in hydrodynamic radius from 33 to 17 nm, which is reasonable for this chain length. A careful look at the data presented by Oostwal[21] shows almost an identical but slightly steeper change for SPS in D_2O by PFGNMR for $M_w = 1.77 \times 10^5$ Da with almost the same diffusion coefficients measured. Ramsay and Schmitz observed[25] a similar 50% increase in the self-diffusion coefficients, in an entirely different 800K Da, 2 mg/mL solution of poly-L-lysine in aqueous solutions for the same range of added KCl. Almost identical results were obtained by Zero and Ware[5] at a slightly different concentration for poly-L-lysine.

These data may also be compared to the scaling predictions of Dobrynin et al.,[29] who have described three regimes of dynamic behavior corresponding to solutions that are dilute, semidilute-unentangled, and semidilute-entangled. Although there is not a wealth of data here to support or contradict these theories, the data where $C_s < C_s^{o-e}$ is consistent with the prediction that D_{self} should be independent of salt concentration in the low salt regime. Above the "o−e transition" the three regimes of polymer concentration provide three different scaling relationships for the dependence of self-diffusion on salt concentration. The three solid lines drawn on Figure 6 above the "o−e transition" have slopes of $^1/_5$, $^1/_2$, and $^5/_4$, representing the predictions for dilute, semidilute-unentangled, and semidilute-entangled solutions, respectively. These data are clearly not evidence of entangled behavior. The slope of the data above the "o−e transition" is between $^1/_5$ and $^1/_2$, and the implication that these chains are not entangled provides a rationale for using the Stokes−Einstein relationship to calculate the hydrodynamic radii above.

Conclusions

The so-called slow mode has been observed at all concentrations of added salt in our work. The independent measurement of self-diffusion by FRAP measurements on our model system of SPS in NMF demonstrates that the slow mode is not self-diffusion as seen by light scattering in semidilute solutions of neutral chains. The results in Figure 6 show that the self-diffusion coefficient is intermediate between the fast and the slow mode at low salt concentrations and is comparable to the fast mode at high salt concentrations, i.e., salt concentrations above the Drifford−Dalbiez ratio.

The gradual increase in the self-diffusion coefficient is an indication that there is no sudden change in chain

conformation associated with the ordinary−extraordinary transition. Ramsay and Schmitz[25] suggest that even in the case of a gradual change, the changes in the observed length scales could not be explained by conformational changes alone. They subscribe to electrolyte dissipation theory by Schurr[30] as a means to explain faster dynamics at increased ionic strength.

References and Notes

(1) Sehgal, A.; Seery, T. A. P. *Macromolecules* **1998**, *31*, 7340−7346.
(2) Amis, E. J.; Han, C. C. *Polymer* **1982**, *23*, 1403−1406.
(3) Lanni, F.; Ware, B. R. *Rev. Sci. Instrum.* **1982**, *53*, 905−908.
(4) Doi, M.; Edwards, S. F. *The Theory of Polymer Dynamics*; Oxford University Press: Oxford, 1986; Vol. 73.
(5) Zero, K.; Ware, B. R. *J. Chem. Phys.* **1984**, *80*, 1610−1616.
(6) Gorti, S.; Plank, L.; Ware, B. R. *J. Chem. Phys.* **1984**, *81*, 909−914.
(7) Smith, L. M.; Smith, B. A.; McConnell, H. M. *Biochemistry* **1979**, *18*, 2256−2259.
(8) Bu, Z.; Russo, P. S. *Macromolecules* **1994**, *27*, 1187−1194.
(9) Cicerone, M. T.; Blackburn, F. R.; Ediger, M. D. *Macromolecules* **1995**, *28*, 8224−8232.
(10) Lodge, T.; Chapman, B. *Trends Polym. Sci. (Cambridge, U.K.)* **1997**, *5*, 122−128.
(11) Leger, L.; Hervet, H.; Rondelez, F. *Macromolecules* **1981**, *14*, 1732−1738.
(12) Wesson, J. A.; Noh, I.; Kitano, T.; Yu, H. *Macromolecules* **1984**, *17*, 782−792.
(13) Yu, H. *Polym. Prepr. (Am. Chem. Soc., Div. Polym. Chem.)* **1991**, *32*, 398−399.
(14) Von Meerwall, E. D.; Amis, E. J.; Ferry, J. D. *Macromolecules* **1985**, *18*, 260−266.
(15) Amis, E. J.; Von Meerwall, E. D.; Ferry, J. D. *Polym. Prepr. (Am. Chem. Soc., Div. Polym. Chem.)* **1987**, *28*, 342−343.
(16) Petit, J. M.; Zhu, X. X.; Macdonald, P. M. *Macromolecules* **1996**, *29*, 70−76.
(17) Furukawa, R.; Arauzlara, J. L.; Ware, B. R. *Macromolecules* **1991**, *24*, 599−605.
(18) Macdonald, P. M.; Uemura, Y.; Dyke, L.; Zhu, X. X. In *Hydrophilic Polymers−Performance with Environmental Acceptance*; Glass, J. E., Ed.; American Chemical Society: Washington, DC, 1996; pp 377−393.
(19) Geschke, D.; Fleischer, G.; Straube, E. *Polymer* **1986**, *27*, 1091.
(20) Oostwal, M.; Odijk, T. *Macromolecules* **1993**, *26*, 6489−6497.
(21) Oostwal, M. G. Rijksuniversiteit te Leiden, Leiden, 1994; p 131.
(22) Composto, R. J.; Kramer, E. J. *J. Mater. Sci.* **1991**, *26*, 2815−2822.
(23) Ewen, B.; Richter, D. In *Neutron Spin−Echo Spectroscopy Viscoelasticity Rheology*; Springer-Verlag: Berlin, 1997; Vol. 134, pp 1−129.
(24) Klepko, V. *Polym. Eng. Sci.* **1999**, *39*, 437−442.
(25) Ramsay, D. J.; Schmitz, K. S. *Macromolecules* **1985**, *18*, 2422−2429.
(26) Yu, K.; Russo, P. S. *J. Polym. Sci., Part B: Polym. Phys.* **1996**, *34*, 1467−1475.
(27) Rabia, I.; Zerouk, J. E.; Mekhalif, S. *Polym. Adv. Technol.* **1998**, *9*, 107−112.
(28) Sohn, D. W.; Russo, P. S.; Davila, A.; Poche, D. S.; Mclaughlin, M. L. *J. Colloid Interface Sci.* **1996**, *177*, 31−44.
(29) Dobrynin, A. V.; Colby, R. H.; Rubinstein, M. *Macromolecules* **1995**, *28*, 1859−1871.
(30) Schurr, M. J. *Chem. Phys.* **1980**, *45*, 119−132.

MA034251E